Journal of Biomolecular NMR **28:** 263–272, 2004.
KLUWER/ESCOM

Triple quantum decoherence under multiple refocusing: Slow correlated chemical shift modulations of C′ and N nuclei in proteins

Julien Wist[a], Dominique Frueh[b], Joel R. Tolman[c] & Geoffrey Bodenhausen[a,d]
[a]*Institute of molecular and biological chemistry, Swiss Federal Institute of Technology Lausanne (EPFL), CH 1015 Lausanne, Switzerland;* [b]*Department of Biological Chemistry and Molecular Pharmacology, Harvard Medical School, 240 Longwood Avenue, Boston, Massachusetts MA 02115, U.S.A.;* [c]*Department of chemistry, John Hopkins University, 3400 N. Charles Street, Baltimore, MD 21218, U.S.A.;* [d]*Département de chimie, associé au CNRS, Ecole Normale Supérieure, 24 rue Lhomond, 75231 Paris cedex 05, France*

Received 4 July 2003; Accepted 30 September 2003

Key words: chemical shift modulations, correlated fluctuations, cross-correlations, protein backbone dynamics, slow motions

Abstract

A new experiment allows the identification of residues that feature slow conformational exchange in macromolecules. Rotations about dihedral angles that are slower than the global correlation time τ_c cause a modulation of the isotropic chemical shifts of the nuclei. If these fluctuations are correlated they induce a differential line broadening between three-spin single-quantum and triple-quantum coherences involving three nuclei such as the carbonyl C′, the neighbouring amide nitrogen N and the amide proton H^N belonging to a pair of consecutive amino acids. A cross-correlated relaxation rate $R_{C'N}^{CS/CS}$ can be determined that corresponds to the sum of the isotropic and anisotropic contributions to the chemical shift modulations of the carbonyl carbon and nitrogen nuclei. Only the isotropic contributions depend on the pulse repetition rate of a multiple-refocusing sequence. An attenuation of the relaxation rate with increasing pulse repetition rate can therefore be attributed to slow motions. The asparagine N25 residue of ubiquitin, located in the first α-helix, is shown to feature significant slow conformational exchange.

Abbreviations: CPMG – Carr-Purcell-Meiboom-Gill; ZQC – Zero-quantum coherence; SQC – Single-quantum coherence; DQC – Double-quantum coherence; TQC – Triple-quantum coherence; CSA – Chemical shift anisotropy; CSM – Chemical shift modulation; CS – Chemical shift.

Introduction

Detailed knowledge of the internal dynamics of biomolecules such as proteins and nucleic acids can contribute to a better understanding of their biological functions. Conformational exchange and local motions span a wide range of time scales from picoseconds to milliseconds. NMR relaxation measurements provide useful tools for the extraction of dynamic information over such a wide range of time scales. A large number of experiments have been reported which allow one to assess fast (ps-ns) motions, using the well-known model-free analysis (Lipari and Szabo, 1982) based on a combination of nitrogen-15 longitudinal, transverse and cross-relaxation rates. Local order parameters S_i^2 can be extracted that provide a measure of local mobility of the i^{th} amino acid or of a fragment thereof. Cross-correlation rates can provide a more refined picture (Pellecchia et al., 1999; Carlomagno et al., 2000; Kumar et al., 2000; Frueh, 2002). In some cases, detailed hypotheses can be made about the precise nature of the motions and sophisticated models can provide a more complete description of dynamic processes (Lienin et al., 1998).

There is growing interest in slow phenomena such as fluctuations of hydrogen bonds and rearrangements of loops, since such motions are thought to be responsible for the specificity of subtle phenomena like

protein complexation with ligands, protein folding, protein/protein and protein/nucleic acid recognition. Slow motions (μs to ms), i.e., motions that are slower than the global tumbling correlation time τ_c, are usually identified by transverse *relaxation dispersion* experiments, i.e., by measuring the dependence of T_2 on the rate $\nu_{CPMG} = 1/(2\tau_{CPMG})$ of a multiple refocusing Carr–Purcell–Meiboom–Gill echo sequence, where τ_{CPMG} is the interval between the centers of two consecutive π pulses, and $2\tau_{CPMG}$ is the cycle period in the sense of average Hamiltonian theory. Alternatively, one can measure the dependence of $T_{1\rho}$ on the effective RF field amplitude in a spin-locking experiment. A decrease of the relaxation rate with increasing pulse repetition rate or RF field amplitude indicates a contribution of slow processes. Recently a number of relaxation dispersion experiments on ^{15}N and ^{13}C single quantum coherences (SQC) have been reported (Mulder et al., 2001; Mills and Szyperski, 2002). However, the complexity of the dynamics hinders a satisfactory characterization of the motions, and further experimental data are required to obtain a more complete picture.

Local motions such as rotations about dihedral angles affect both anisotropic and isotropic components of the chemical shifts. *Ab initio* calculations have shown that the isotropic component of the chemical shift tensor of a nucleus $\sigma_{iso} = \frac{1}{3}(\sigma_{xx} + \sigma_{yy} + \sigma_{zz})$ is sensitive to subtle changes of conformations in the vicinity of the nucleus (Arnold and Oldfield, 2000; Brender et al., 2001). Motions that are slower than the correlation time τ_c of the molecule can lead to a modulation of the isotropic shifts of neighbouring nuclei, and thus contribute to the relaxation of coherences. By contrast, the anisotropic components (CSAs) are averaged out by overall tumbling in the intervals between rare conformational rearrangements. Multiple quantum coherences (MQCs) will not only be sensitive to the fluctuations of the chemical shifts of the nuclei involved in the coherences, but also to cross-correlation between the modulations of their chemical shifts (CSM/CSM). Since these interferences affect zero quantum coherences (ZQCs) and double quantum coherences (DQCs) in a different manner, the difference between their relaxation rates allows one to determine the cross-correlation rates (Pellecchia et al., 1999; Kloiber and Konrat, 2000; Pervushin, 2001). Initial reports on CSM/CSM effects have shown that they can be observed for donor and acceptor nitrogen-15 nuclei in nucleic acids (Chiarparin et al., 2001) and

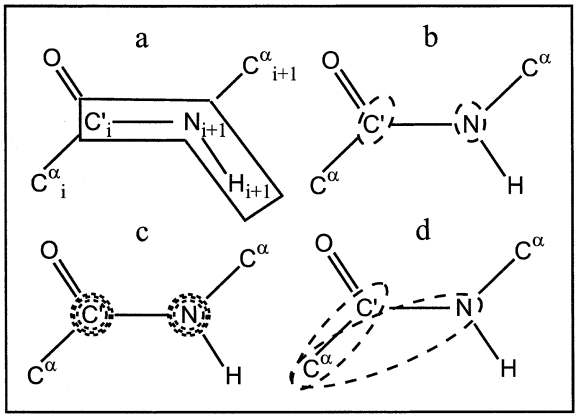

Figure 1. (a) Three-spin single-quantum coherence SQC ($C'_{\pm}N_{\mp}H^N_{\pm}$) and triple-quantum coherence TQC ($C'_{\pm}N_{\pm}H^N_{\pm}$) in neighbouring amino acids in proteins. (b) CSA/CSA cross-correlation due to concerted modulations of the anisotropic chemical shifts (represented by ellipses), (c) CSM/CSM cross-correlation due to concerted fluctuations of the isotropic parts of the chemical shifts (dotted circles), (d) Dipole/dipole interference involving an external spin (in this case C^{α}_i). Such mechanisms contribute to auto-relaxation of the three-spin SQC and TQC, induce differential line broadening, and cannot be averaged out using non-selective π-pulses.

for C^{α} and C^{β} nuclei in side-chains of proteins (Frueh et al., 2001; Vugmeyster et al., 2003).

Unfortunately, fluctuations of isotropic (CSM) and anisotropic (CSA) components of the chemical shifts affect ZQC's and DQC's in the same way. The measured rate is therefore a sum of two contributions as sketched in Figures 1b and 1c. We propose to use the notation:

$$R^{CS/CS} = R^{CSA/CSA} + R^{CSM/CSM}, \qquad (1)$$

where the former term is sensitive to overall tumbling and fast internal motions, while the latter is only significant in the presence of internal motions that are slower than the correlation time τ_c. The experiments described in this paper allow one to measure the $R^{CS/CS}_{C'/N}$ cross-correlation rate of MQC's as a function of the rate $\nu_{CPMG} = 1/(2\tau_{CPMG})$. The $R^{CSM/CSM}$ contributions due to the isotropic components decrease with increasing pulse repetition rate, while the $R^{CSA/CSA}$ contributions are not affected. This enables unambiguous identification of residues experiencing slow conformational exchange.

Materials and methods

Uniformly $^{13}C/^{15}N/^{2}D$-enriched ubiquitin was obtained commercially (VLI). The protein was dissolved

in 10% D_2O/90% H_2O with phosphate buffer at pH 6.7 to a concentration of 1.5 mM. NMR data were acquired at 300 K on a 600 MHz Bruker DMX spectrometer equipped with a quadruple resonance TBI probe and three orthogonal gradient coils. For each 2D spectrum 64 × 512 complex points were recorded using the pulse sequence shown in Figure 2. The spectral widths were 1520 and 8389 Hz in the ω_1 and ω_2 dimensions. For each t_1 increment 32 scans were accumulated with a relaxation delay of 3 s, optimized to take account of the slow longitudinal relaxation of amide protons in an otherwise deuterated protein. The total acquisition time for each 2D experiment was 1.7 h. Processing of the data was performed using the GNU Package NmrPipe/NmrDraw/NlinLS (Delaglio et al., 1995). Each dimension was apodized by a 90° phase-shifted squared sine-bell window function and zero-filled once. Relaxation rates were obtained by least-squares fitting of the decay curves to exponential functions. Dispersion curves of relaxation rates as a function of $\nu_{CPMG} = 1/(2\tau_{CPMG})$ were fitted with a Matlab script (Matlab, 1992). Errors were estimated by a Monte-Carlo analysis using 300 synthetic data sets.

The pulse sequence shown in Figure 2 is designed to measure the decays of single- and triple-quantum coherences SQC ($C'_{\pm}N_{\mp}H^N_{\pm}$) and TQC ($C'_{\pm}N_{\pm}H^N_{\pm}$) (see Figure 1a). The preparation period allows one to transfer the amide proton magnetization H^N_z into doubly antiphase single quantum coherence SQC ($4C'_zN_xH^N_z$) at point (a). A z-filter is applied to the three-spin order term $4C'_zN_zH^N_z$ at (b) and three simultaneous rectangular $\pi/2$-pulses create either $4C'_yN_xH^N_y$ or $4C'_xN_yH^N_y$ at (c), i.e., combinations of single- and triple-quantum coherences. We are however only interested in mechanisms that involve C′ and N nuclei. We shall speak of pseudo ZQC ($C'_+N_-H^N_{\pm} \pm C'_-N_+H^N_{\mp}$) and pseudo DQC ($C'_+N_+H^N_{\pm} \pm C'_-N_-H^N_{\mp}$) operators. In order to separate these two terms, only nitrogen and carbon excitation pulses need to be phase cycled, since the proton coherence order is irrelevant in the present study as may be appreciated from the toggling frame diagrams in Figure 3.

Applying long pulse trains simultaneously to the carbon and nitrogen nuclei can lead to heating of the probe. Therefore, low-power RF pulses are used during the mixing time τ_m (in square brackets in Figure 2) to refocus the chemical shifts and J-couplings that affect the three-spin coherence, and to separate the desired CS/CS cross-correlation rate $R_{C'N}$ from other undesirable cross-correlated rates $R^{DD/DD}$, $R^{CS/DD}$ and $R^{CS/CS}$ involving $C'_i-C^{\alpha}_i$, $N_{i+1}-H^N_{i+1}$, $N_{i+1}-C^{\alpha}_{i+1}$, $C^{\alpha}_i-H^N_{i+1}$ dipole-dipole interactions on the one hand and C'_i, N_{i+1} and H^N_{i+1} CSA tensors on the other. This is achieved by simultaneously refocusing the carbon and nitrogen nuclei and by inverting the protons in the center of each $\frac{1}{2}\tau_{CPMG}$ delay, as shown in Figure 3 using a description in terms of toggling frames (Chiarparin et al., 1999). Only cross-correlated CS/CS interference involving C′ and N nuclei contributes to differential line broadening between the two selected sets of operators.

After the relaxation interval τ_m in Figure 2, a z-filter is again applied to the three-spin order $4C'_zN_zH^N_z$ to suppress phase distortions resulting from changes in RF field amplitudes and to eliminate any spurious coherences (Sørensen et al., 1984). During the subsequent evolution period t_1 the magnetization is labelled by the ^{15}N chemical shifts in a semi-constant time fashion (Logan et al., 1993) and transferred back to the amide protons using the sensitivity enhancement technique (Palmer et al., 1991; Kay et al., 1992). Solvent suppression is achieved using a selective flip-back pulse (Grzesiek and Bax, 1992) combined with gradient selection.

Results and discussion

Differential line-broadening, i.e., the difference between the decay rates of pseudo ZQC ($C'_+N_-H^N_{\pm} \pm C'_-N_+H^N_{\mp}$) and pseudo DQC ($C'_+N_+H^N_{\pm} \pm C'_-N_-H^N_{\mp}$) operators, arises from a combination of auto-correlated (AC) and cross-correlated (CC) interference effects. The π-pulses applied during the mixing time τ_m allow one to cancel the effects of most undesired relaxation mechanisms (see Figure 3). Some mechanisms can unfortunately not be rejected in this manner and their rates have to be estimated. For a three-spin coherence, three auto-correlated dipole-dipole mechanisms between spins that are actively involved, $C'_i-N_{i+1}/C'_i-N_{i+1}$, $C'_i-H^N_{i+1}/C'_i-H^N_{i+1}$ and $N_{i+1}-H^N_{i+1}/N_{i+1}-H^N_{i+1}$ contribute to differential line broadening. None of the dipolar contributions are proportional to J(0) for pseudo ZQC and DQC terms. For ubiquitin in the rigid limit ($S^2 = 1$) at room temperature ($\tau_c = 4$ ns) and 14 T ($\omega_H/2\pi = 600$ MHz), their contributions, estimated to be $1.1 \cdot 10^{-3}$, $1.8 \cdot 10^{-3}$ and $3.5 \cdot 10^{-2}$ s^{-1}, can be neglected. Moreover, by including the amide proton into the three-spin coherence (Pelluchia et al., 1999),

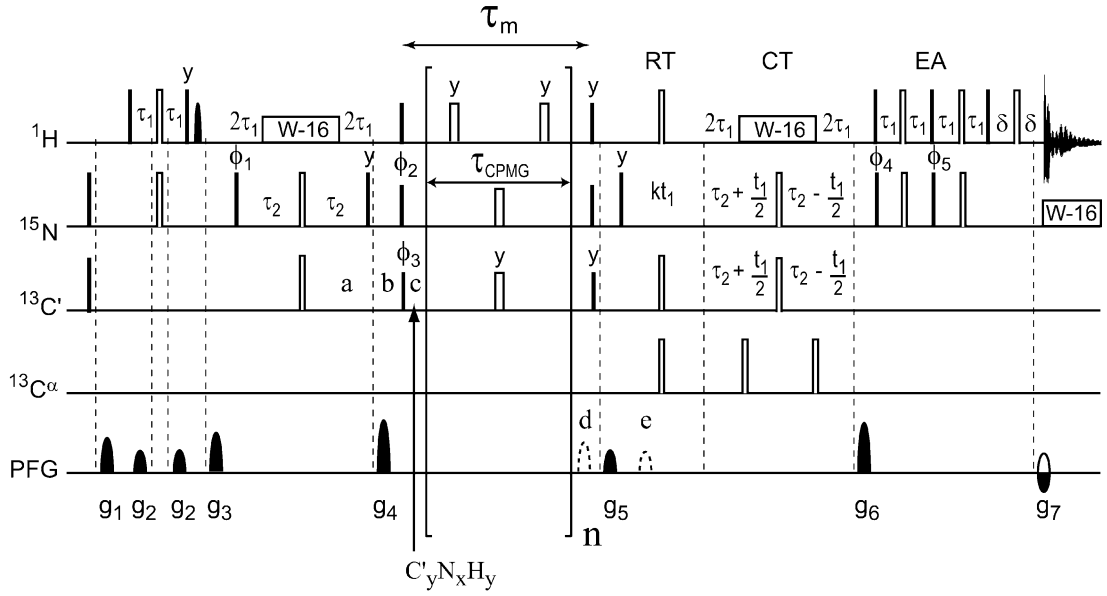

Figure 2. Pulse sequence designed to measure the auto-relaxation of three-spin pseudo ZQC ($C'_+N_-H^N_\pm \pm C'_-N_+H^N_\mp$) and pseudo DQC ($C'_+N_+H^N_\pm \pm C'_-N_-H^N_\mp$) operators. Black and white rectangles represent π/2 and π pulses. All pulses are applied along the x axes, unless specified otherwise. The ^{1}H, ^{15}N, ^{13}C carriers are centered at 4.7, 118 and 175 ppm, respectively. 90° and 180° pulses are applied to ^{13}C with field strengths of $\Delta/\sqrt{15}$ and $\Delta/\sqrt{3}$, Δ being defined as the difference in Hz between the centers of the C′ and C^α regions (Δ = 17.6 kHz at 600 MHz). Pulses applied to C^α are phase modulated. During the mixing time τ_m, the evolution of the three-spin coherence is refocused by two simultaneous rectangular pulses of identical duration (4.5 kHz, 110 μs) applied to ^{13}C and ^{15}N in the middle of τ_{CPMG} and by two (14 kHz, 35 μs) rectangular proton pulses applied at $1/4\tau_{CPMG}$ and $3/4\tau_{CPMG}$. The delays are set to $\tau_1 = 2.7$ ms ($\approx 1/4J(NH)$), $\tau_2 = 15.1$ ms ($\approx 1/4J(C'N)$), and $\delta = 1.3$ ms. The ^{15}N magnetization evolves during a semi-constant time period comprised of two intervals RT (real time) and CT (constant time). Quadrature detection is achieved in ω_1 by the enhanced-sensitivity pulsed field gradient method. WALTZ-16 sequences are used to perform proton and nitrogen decoupling with RF field strengths of 3.5 kHz and 1.2 kHz, respectively. The phase cycle (16 steps) is $\phi_1 = 8(x,-x)$, $\phi_2 = 4(y),4(-x),4(-y),4(x)$, $\phi_3 = 4(x),4(y),4(-x),4(-y)$, $\phi_4 = 4(x,x,-x,-x)$, $\phi_5 = 4(y,y,-y,-y)$. For the selection of pseudo DQC or pseudo ZQC, $\phi_{rec} = 4(x,-x,-x,x)$ or $\phi_{rec} = 2(x,-x,-x,x,-x,x,x,-x)$, respectively. The identity of these terms has been verified by inserting (optional) gradient pulses at points (d) and (e) with suitable amplitude ratios. This allows one to verify that the dephasing and refocusing correspond to coherences involving nuclei with gyromagnetic ratios of opposite signs. The duration of all sine-shaped gradients is 1 ms and their peak amplitudes are $g_{1x} = 31$ G/cm, $g_{2y} = 20$ G/cm, $g_{3z} = 19.5$ G/cm, $g_{4x} = 45$ G/cm, $g_{5z} = 30$ G/cm, $g_{6z} = 39.5$ G/cm, $g_{7z} = -4$ G/cm.

one can avoid cross-correlation effects due to dipole-dipole interactions $C'_i{-}H^N_{i+1}/N_{i+1}{-}H^N_{i+1}$, expected to be up to 0.8 s^{-1} in our case. In deuterated proteins, other dipolar interactions are negligible. Finally, the DD/DD interferences $C'_i{-}C^\alpha_i/N_{i+1}{-}C^\alpha_i$ or $C'_i{-}C^\alpha_{i+1}/N_{i+1}{-}C^\alpha_{i+1}$ involving an external C^α nucleus and the C'_i and N_{i+1} nuclei participating in the MQC (see Figure 1) can safely be neglected: in our case, the resulting contributions are estimated to be ≤ 0.025 s^{-1}. As a result, only two cross-correlated mechanisms, CSA/CSA and CSM/CSM (Figures 1b and 1c), contribute significantly (and with opposite signs) to the auto-relaxation rates. Their difference $\Delta R^{(AR)}{=}R^{(AR)}$(pseudo-DQC)$-R^{(AR)}$ (pseudo-ZQC) is:

$$\Delta R^{(AR)} = 2R^{CS/CS}_{C'N} = 2(R^{CSA/CSA}_{C'N} + R^{CSM/CSM}_{C'N}). \quad (2)$$

Slow motions and chemical shift modulations. Chemical shift modulations, which cause the Hamiltonian to be time-dependent, are equivalent to chemical exchange and can therefore be treated using well-known exchange theory. The Hamiltonian of the system can be described by a time-independent part H_0 and a stochastic perturbation H_1 due to the chemical shift modulation (Deverell et al., 1970; Wennerström, 1972):

$$H(t) = H_0 + H_1^{CSM}(t), \quad (3)$$

where $H_1^{CSM}(t)$ is defined by:

$$H_1^{CSM}(t) = \sum_i \delta\omega_i(t) I_{zi}, \quad (4)$$

where the factors $\delta\omega_i(t)$ represent the time-dependent deviations from the average chemical shifts ω_i, so that $< \delta\omega_i(t) >= 0$, and the summation must be carried

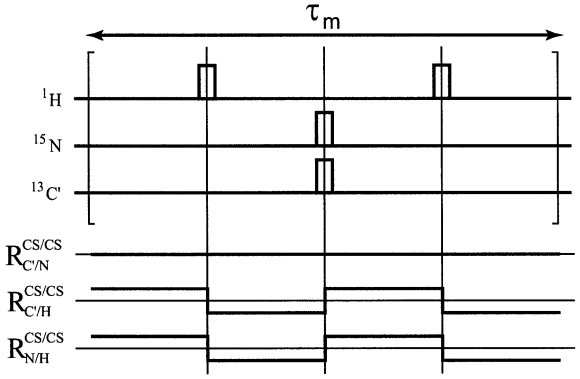

Figure 3. Toggling frame diagrams showing how different cross correlation rates can be selected or eliminated by suitable positioning of π pulses. We focus attention on the three mechanisms $R^{CS/CS}_{C'/N}$, $R^{CS/CS}_{C'/H}$ and $R^{CS/CS}_{N/H}$. The first of these remains invariant, whereas the latter two change sign and are therefore averaged out. Similar averaging leads to the elimination of various dipolar terms involving C^{α}. The timing of the pulses can easily be modified to select the second or third rate.

out over all nuclei I_i that are involved in the multiple-quantum coherence. Assuming instantaneous jumps, the isotropic contributions $R_2^{CSM/CSM}$ to the transverse auto-relaxation rate of a coherence represented by a product operator B_S may be expressed as:

$$R_2^{CSM/CSM}(B_S) = \sum_{m,n} R_{m,n}^{CSM/CSM} = \frac{1}{2}\sum_{m,n} J_{m,n}^{CSM/CSM}(0)\frac{\langle B_s|[I_{zm},[I_{zn},B_s]]\rangle}{\langle B_s|B_s\rangle}, \quad (5)$$

where the indices m and n run over all nuclei involved in the multiple-quantum coherence B_S. The spectral density $J_{m,n}^{CSM/CSM}(0)$ provides a measure of the correlation between the fluctuations of the isotropic chemical shifts associated with these nuclei:

$$J_{m,n}^{CSM/CSM}(0) = \int_{-\infty}^{+\infty} \overline{\delta\omega_m(t)\delta\omega_n(t+\tau)}d\tau \quad (6)$$

An interesting feature of Equation 6 is that if $m \neq n$ the spectral density can take negative values when the chemical shift modulations are anti-correlated (Frueh, 2002). Longitudinal magnetization does *not* relax under CSM since all operators I_{zn} commute with Zeeman order I_{zs} and with longitudinal two-spin order terms such as $2I_{zr}I_{zs}$. The prediction of the average in Equation 6 requires a model of the motions. Usually, one considers fluctuations between two conformations A and B assuming instantaneous jumps. If we further assume that the two nuclei are affected simultaneously by the same exchange event one can evaluate Equation 5 as a function of the exchange lifetime k_{ex} by adapting the equation for single-quantum line broadening (Wennerström, 1972):

$$R_{m,n}^{CSM/CSM} = 2p_A p_B \Delta\omega_m^{AB}\Delta\omega_n^{AB}\frac{1}{k_{ex}}, \quad (7)$$

where k_{ex} is the sum of the forward and backward exchange rates k_+ and k_-, p_A and p_B represent the populations of sites A and B, and $\Delta\omega_m^{AB}$ and $\Delta\omega_n^{AB}$ are the differences in chemical shifts of spins m and n between sites A and B ($\Delta\omega_m^{AB} = \omega_m^A - \omega_m^B$, $\Delta\omega_n^{AB} = \omega_n^A - \omega_n^B$). The factor two in Equation 7 arises from the fact that both $[I_{zm},[I_{zn},B_s]]$ and $[I_{zn},[I_{zm},B_s]]$ contribute to the cross-correlated relaxation rates $R_{m,n}^{CSM/CSM}(B_S)$ in Equation 5 (Kloiber and Konrat, 2000).

Decay rates measured with a single refocusing pulse. Figure 4 shows the difference between the decay rates of three-spin pseudo ZQC ($C'_+N_-H^N_{\pm} \pm C'_-N_+H^N_{\mp}$) and pseudo DQC ($C'_+N_+H^N_{\pm} \pm C'_-N_-H^N_{\mp}$) operators, for all observable residues, measured with one hard refocusing π-pulse applied to carbon-13 (10 kHz, 49 μs) and one to nitrogen-15 (12.5 kHz, 39 μs) during the mixing time ($n = 1$ in Figure 2). Out of 64 observable residues in ubiquitin, 8 were excluded from the analysis because of overlapping signals: E16, V26, Q31, D39, R42, S57, L71 and R72. Residue T12 was excluded from the final analysis since its poor signal-to-noise ratio led to large errors. The measured CS/CS cross-correlation rates shown in Figure 4 are generally between -2.5 and $+2$ s^{-1} which agrees with predictions of the CSA/CSA contributions (open squares and diamonds), calculated using the X-ray structure (Vijay-Kumar et al., 1987) and assuming the structure to be rigid, i.e., $S^2 = 1$. Open diamonds were estimated using ^{13}C and ^{15}N CSA tensors (Bax and Cornilescu, 2000) averaged over all residues, while open squares were evaluated using different tensors depending on the environment (α-helices or β-sheets) in the protein. For most residues, the predicted CSA/CSA contributions can account for the experimental rates, but the behaviour of asparagine N25 can only be understood if one postulates a significant correlated CSM/CSM modulation of the isotropic chemical shifts in order to account for the negative experimental rate $R^{CS/CS} = -6.8$ s^{-1}. The predicted rate $R^{CSA/CSA}$ is between -2.5 s^{-1} and -1.5 s^{-1} for this residue depending on the CSA tensors used in the calculations.

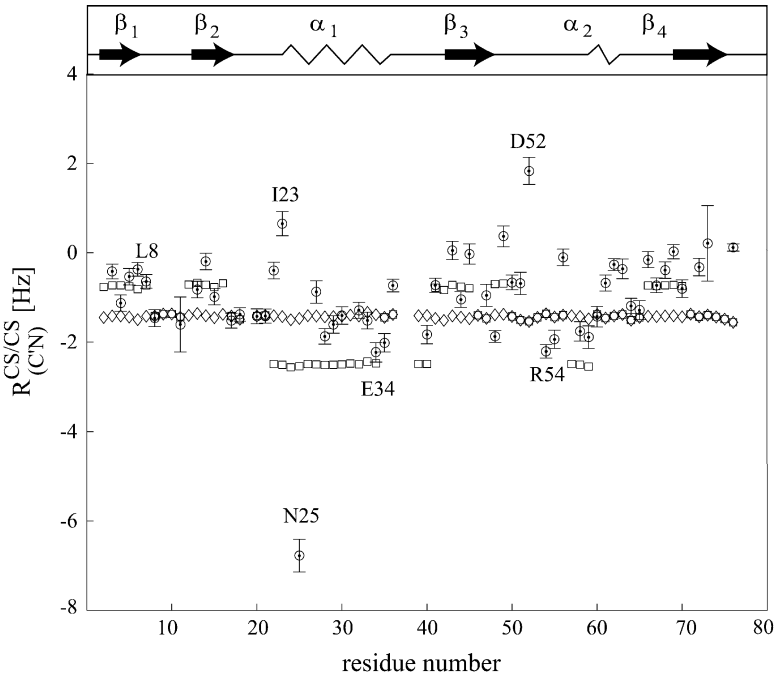

Figure 4. Cross-correlated relaxation rates $R^{CS/CS}_{C'N}$ vs. residue number in ubiquitin. Dots with error bars represent experimental values measured with a single refocusing pulse during the mixing time (see text). Open diamonds and squares correspond to predicted values of $R^{CSA/CSA}_{C'N}$. Bond angles were calculated from the X-ray structure of ubiquitin. The order parameter S^2 was assumed to be 1 (rigid limit). Diamonds indicate rates that were calculated assuming average anisotropic ^{13}C and ^{15}N CSA tensors for all residues with an angle $\beta_C = 38°$ between the unique axis of the ^{13}C CSA tensor and the C′N bond vector and an angle $\beta_N = 19°$ between the unique axis of the ^{15}N CSA tensor and NH bond vector. Open squares were calculated assuming different ^{13}C and ^{15}N CSA tensors and angles for β-strands ($\beta_C = 37°$ and $\beta_N = 19°$) and α-helices ($\beta_C = 42°$ and $\beta_N = 16°$).

Decay rates measured with multiple refocusing. To separate the CSM/CSM contributions from the CSA/CSA rates, relaxation dispersion curves were obtained by repeating the experiment with $n = 2, 4, 6, \ldots, N$ for pulse intervals τ_{CPMG} = 0.8, 2.4, 4, 6, 6.8, 8, 10, 12 and 14 ms. Fitting the experimental decays, which are nearly mono-exponential for each τ_{CPMG} interval, allows one to extract the auto-relaxation rates R^{AR}(pseudo-ZQC) and R^{AR}(pseudo-DQC), and hence to evaluate the cross-correlation rates $R^{CSM/CSM}_{m,n}$ for each residue and for each τ_{CPMG} interval. Figure 5 shows such curves for the asparagine N25 residue. Clearly an attenuation of the rates is observed: The relaxation rate drops from ca. $-6\ s^{-1}$ (slow pulse repetition rate) to about $-1\ s^{-1}$ (fast pulse repetition rate). This is in agreement with other studies showing that N25 is subject to conformational exchange (Lienin et al., 1998; Mills and Szyperski, 2002).

In the limit of fast exchange $\Delta\omega^{AB}_{m,n}\tau_{ex} \ll 1$, the dependence of the measured relaxation rates on the frequency $\nu_{CPMG} = 1/(2\tau_{CPMG})$ can be obtained by extending the general equation (Luz and Meiboom, 1963) if $T_{2A} = T_{2B} = T_2$:

$$R^{CSM/CSM}_{m,n} = 2p_A p_B \Delta\omega^{AB}_m \Delta\omega^{AB}_n \frac{1}{k_{ex}} \left[1 - \frac{2\tanh(k_{ex}\tau_{CPMG}/2)}{k_{ex}\tau_{CPMG}}\right]. \quad (8)$$

The term in the square brackets can vary from 0 (for $k_{ex} \ll 1/(2\tau_{CPMG})$) to 1 (for $k_{ex} \gg 1/(2\tau_{CPMG})$). In the limit of very slow pulse repetition rates, both isotropic and anisotropic contributions participate to differential line-broadening, while for very fast pulse repetition rates only the CSA/CSA interferences remain. Moreover, fitting the relaxation dispersion curves to Equation 8 allows one to extract the two parameters k_{ex} and $p_A p_B \Delta\omega^{AB}_m \Delta\omega^{AB}_n / 4\pi^2$.

For very slow motions and very unequal populations, it may be necessary to use more general equations (Allerhand and Gutowsky, 1965; Carver and Richards, 1972; Davis et al., 1999; Ishima and

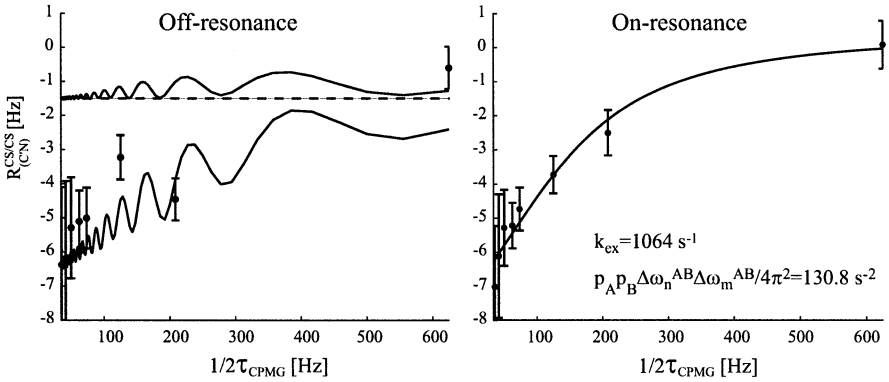

Figure 5. Relaxation dispersion curves for asparagine N25 in ubiquitin, showing the apparent rate $R^{CS/CS}_{C'N}$ as a function of the Carr–Purcell–Meiboom–Gill rate $\nu_{CPMG} = 1/(2\tau_{CPMG})$. Dots with error bars represent experimental data. On the left: the upper solid curve represents the simulated dispersion curve without chemical shift modulation ($p_A p_B \Delta\omega_m^{AB} \Delta\omega_n^{AB}/4\pi^2 = 0$) and the lower solid curve with chemical shift modulation ($k_{ex} = 1064\ s^{-1}$ and $p_A p_B \Delta\omega_m^{AB} \Delta\omega_n^{AB}/4\pi^2 = 130.8\ s^{-2}$) affecting simultaneously the carbon and nitrogen nuclei (as explained in the text). The dashed line represents the constant $R^{CSA/CSA}_{C'/N}$ cross-correlation rate used in the simulations. On the right: Experimental rates obtained for asparagine N25 when the carrier frequencies are set on-resonance for each nucleus involved in the coherence during the Carr–Purcell sequence. In this case, no oscillations are observed. The solid curve represents the fit using Equation 8.

Torchia, 1999) and investigate the dependence of the relaxation rates on the static field (Millet et al., 2000).

Oscillations due to offset effects. The left-hand side of Figure 5 shows the experimental decay rates (dots with error bars) plotted as a function of the pulse repetition rate. The oscillations can be attributed to offset effects (tilted effective fields) during the Carr–Purcell–Meiboom–Gill sequence. Because the refocusing pulse trains are applied to all three nuclei involved in the coherence, three offsets must be considered that can interfere together. The accurate analysis of relaxation during an imperfect CPMG sequence requires numerical simulations. Such simulations were performed using Matlab, by propagating the full Liouvillian starting with an initial two-spin coherence $2C'_yN_x$ (neglecting the proton to reduce the dimensions of the Liouville space to 16 × 16) during several cycles $n = 2, 4, 6, \ldots$ of the Carr–Purcell sequence, each cycle consisting of $[\tau_{CPMG}/2 - \pi - \tau_{CPMG}/2]$. The operator basis of a two-spin system consists of 15 operator products in addition to the unity operator. The corresponding Liouville equations can therefore be written using a 15 × 15 matrix and a 15-dimensional vector describing the density operator elements. A 30 × 30 matrix is required to write the McConnell equations for two sites A and B (2 × 15 operators) (Helgestrand et al., 2000). Assuming dynamic equilibrium, this leads to a 31 × 31 matrix where the first column corresponds to the equilibrium magnetization. The homogeneous McConnell equation is:

$$\frac{d}{dt}\sigma(t) = -P\sigma(t), \tag{9}$$

where the superoperator P is represented by a 31 × 31 matrix and σ by a 31-dimensional vector. Since P does not depend on time during the interval Δt, the solutions of this differential equation are:

$$\sigma(t + \Delta t) = exp\,[-P\Delta t]\,\sigma(t). \tag{10}$$

After n cycles ($t = n\tau_{CPMG}$) the expectation values $\langle 2C_yN_x(A)\rangle$ and $\langle 2C_xN_y(A)\rangle$ for site A are given by the scalar products:

$$\begin{aligned}\langle 2C_yN_x(A)\rangle &= \langle \sigma(n\tau_{CPMG})|2C_yN_x(A)\rangle \\ \langle 2C_xN_y(A)\rangle &= \langle \sigma(n\tau_{CPMG})|2C_xN_y(A)\rangle\end{aligned} \tag{11}$$

and likewise for site B. The expectation values of ZQC ($C_\pm N_\mp(A)$) and DQC ($C_\pm N_\pm(A)$) were evaluated by combining the cartesian expectation values in an adequate manner. The resulting mono-exponential decays were fitted to extract the CS/CS cross-correlation rates, which were plotted as a function of the rate $\nu_{CPMG} = 1/(2\tau_{CPMG})$.

The carbon and nitrogen offsets observed for N25 in a three-dimensional HNCO experiment ($\omega_{C'}/2\pi = 251.2$ Hz and $\omega_N/2\pi = 171.8$ Hz) were used in the simulations of the off-resonance decays. Other parameters used in the simulations were similar to those of the experiment described in Figure 2. On the left-hand side of Figure 5, the dashed line represents

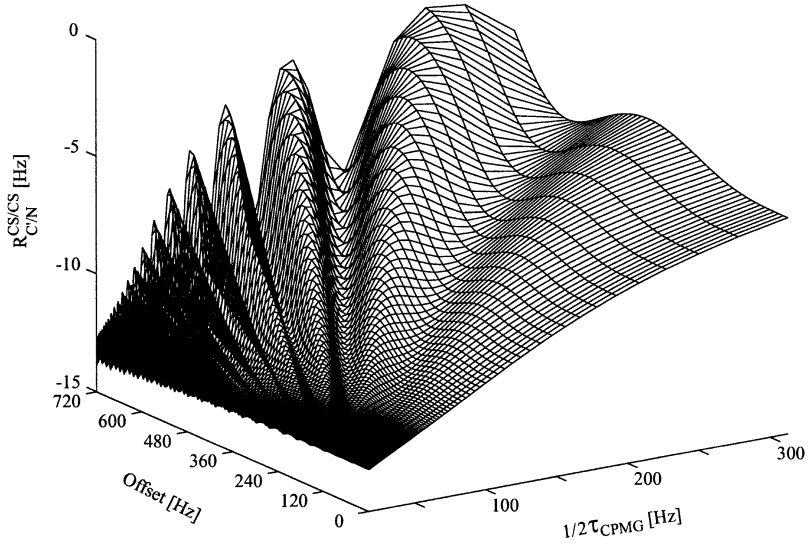

Figure 6. Simulated dispersion curves as function of the offset of the amide nitrogen. The pulses are of same duration for both nuclei (5 kHz, 100 μs), and the ^{13}C offset is set to zero. Significant distorsions can already be observed at an offset of 360 Hz (6 ppm) that corresponds to a quarter of the spectral width commonly observed for amide nitrogens at 14 T.

the constant anisotropic contribution $R_{C'/N}^{CSA/CSA}$ to the cross-correlation rate, i.e., the rate that remains if the CSM/CSM contributions are negligible or have been eliminated by rapid refocusing ($k_{ex} \ll 1/(2\tau_{\mathrm{CPMG}})$). The two solid lines on the left-hand side represent simulated relaxation dispersion curves calculated with the parameters given in the legend.

Since the simulations were for a two spin-system, the simulated profiles on the left-hand side of Figure 5 should *not* be considered as fits of our experimental data, but merely as a demonstration of possible effects induced by offsets when a Carr–Purcell sequence is applied to a multiple quantum coherence. In the experiments, the proton offsets will also contribute to the modulation of the relaxation dispersion curve. Yet for the sake of simplicity, the simulations were not extended to triple quantum coherence. The simulations clearly underscore the fact that the attenuation of the cross-correlation rate $R_{\mathrm{C'N}}^{\mathrm{CS/CS}}$ as a function of $\nu_{\mathrm{CPMG}} = 1/(2\tau_{\mathrm{CPMG}})$ is really due to the presence of conformational exchange rather than to artifacts.

Decay rates measured with multiple refocusing using on-resonance pulses. For a selected amino acid, it is possible to repeat the experiments with all three carrier frequencies (i.e., those of the carbon-13, nitrogen-15 and proton channels) positioned on-resonance during the Carr–Purcell–Meiboom–Gill sequence. We shall focus attention on the asparagine N25 residue that appears to have an unusual dynamic behaviour (see Figure 4). For this residue, no oscillations were observed in the on-resonance relaxation dispersion curves. The right-hand side of Figure 5 shows the experimental data points. Fitting the dispersion curve to Equation 8 assuming fast exchange allows us to extract the parameters $k_{ex} = 1064\ \mathrm{s}^{-1}$ and $p_A p_B \Delta\omega_m^{AB} \Delta\omega_n^{AB}/4\pi^2 = 130.8\ \mathrm{s}^{-2}$. Conformational exchange in macromolecules sometimes violates the fast exchange approximation, i.e., $\Delta\omega_{m,n}^{AB}\tau_{ex}$ may not be small, and the fact that only one line is observed for a two-site exchange system does not necessarily allow one to assume that the conditions for fast exchange are fulfilled. Indeed, if $p_A \ll p_B$ only a single line may be observed since the other one may be very weak. However, our analysis suffices to identify residues that are subject to conformational exchange. The presence of significant isotropic (CSM/CSM) contributions, suggested by the large discrepancy between the predicted CSA/CSA contributions and the measured CS/CS rates, is clearly confirmed by the drastic attenuation of the relaxation rates with increasing pulse repetition rates. Repeating this experiments at different static fields B_0 should permit a better characterization of the motions (Millet et al., 2000).

If the offsets are not vanishingly small compared to the RF amplitudes, oscillations appear that are due to tilted effective fields, as illustrated in Figure 6, which make it difficult to extract reliable decay rates.

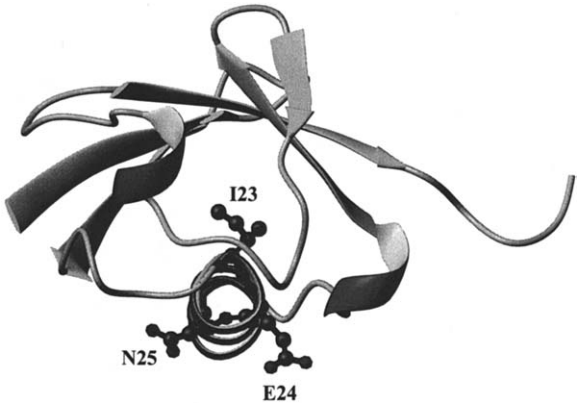

Figure 7. Ribbon representation of an X-ray structure of ubiquitin (1ubq.pdb). The highly mobile arginine N25 residue and its neighbours glutamic acid E24 and isoleucine I23 are shown. The figure was made with MOLMOL.

Thus two-dimensional NMR cannot be used in an effective manner with multiple refocusing (n > 1). Further research is under way to evaluate the performance of triple-resonance CPMG sequences that use frequency-swept adiabatic 'chirp' pulses for both carbon-13 and nitrogen-15 nuclei. Chirp pulses can be made weak enough to avoid heating effects, yet allow one to refocus three-spin SQC and TQC over wide ranges of offsets. If broad-band methods fail, it would be preferable to use selective methods to investigate one residue after another. One possible method would use a transfer by selective cross-polarization (Ferrage et al., 2000, 2003) from protons to nitrogen-15 prior to the excitation of longitudinal three-spin order $4C'_z\mathrm{N}_z\mathrm{H}^{\mathrm{N}}_z$. After SQC or TQC relaxation and evolution of SQC under the nitrogen-15 chemical shifts, a second transfer by selective cross-polarization would generate observable proton magnetization. If the dynamic properties of only a few residues need to be characterized, this would allow one to reduce considerably the experimental time.

Conclusions

We have presented a new approach to identify unambiguously the presence or absence of slow motions in the backbone of a biomolecule. Motions that are slower than the global correlation time τ_c can lead to correlated modulations of the isotropic components of the chemical shifts. The relaxation rates of three-spin single- and triple-quantum coherences therefore depend on the pulse repetition rate of Carr–Purcell–Meiboom–Gill multiple refocusing sequences, an effect known as relaxation dispersion. If fast pulse repetition rates lead to longer decays, i.e., to a decrease of the apparent relaxation rates, this can be attributed to the presence of slow conformational exchange. This effect can be caused by correlated or anticorrelated fluctuations of the isotropic chemical shifts. In ubiquitin it was possible to confirm the presence of pronounced local mobility of the asparagine N25 residue, which is in agreement with previous work (Lienin et al., 1998; Mills and Szyperski, 2002). The simple observation that the resonance of the neighbouring glutamic acid residue E24 is strongly attenuated in the HSQC spectrum, and the fact that the next residue towards the beginning of the first α-helix, isoleucine I23, has an abnormally fast $\mathrm{N/H}^N$ cross-correlated CSM/CSM relaxation rate (as observed when the experiment is modified to focus attention on the correlation of the slow modulations of the isotropic chemical shifts of the N and H^N nuclei, see Figure 3) tend to indicate the presence of local motions in this exposed part of the protein.

Preliminary research in our laboratory indicates that the TQC experiment can reveal changes in internal mobility of proteins upon complex formation. Specifically, we have compared CSM/CSM relaxation rates in Major Urinary Protein (MUP) that is either bound to a pyrazine derivative (a model for a pheromone) or in its free 'apo' form. Earlier studies of the apo and bound forms of this carrier protein (Zidek et al., 1999) that use a conventional model-free analysis (Lipari and Szabo, 1982) of single-quantum nitrogen-15 relaxation show only very subtle changes. By contrast, the TQC experiment described in this paper allowed us to identify significant changes in internal mobility between apo and bound forms of the protein. Thus the method provides a useful tool for characterizing slow dynamics in macromolecules.

Acknowledgements

We are indebted to Martial Rey for his invaluable technical assistance. This research was supported by the Fond National de la Recherche Scientifique and by the Commission pour la Technologie et l'Innovation.

References

Allerhand, A. and Gutowsky, H.S.: 1965, *J. Chem. Phys.*, **41**, 1587–1599.

Arnold, W.D. and Oldfield, E.: 2000, *J. Am. Chem. Soc.*, **122**, 12835–12841.
Bax, A. and Cornilescu, G.: 2000, *J. Am. Chem. Soc.*, **122**, 10143–10154.
Brender, J.R., Taylor, D.M. and Ramamoorthy, A.: 2001, *J. Am. Chem. Soc.*, **123**, 914–922.
Carlomagno, T., Maurer, M. Hennig, M. and Griesinger, C.: 2000, *J. Am. Chem. Soc.*, **122**, 5105–5113.
Carver, J.P. and Richards, R.E.: 1972, *J. Magn. Reson.*, **6**, 89–105.
Chiarparin, E., Pelupessy, P., Ghose, R. and Bodenhausen, G.: 1999, *J. Am. Chem. Soc.*, **121**, 6876–6883.
Chiarparin, E., Rüdisser, S. and Bodenhausen, G.: 2001, *ChemPhysChem.*, **2**, 41–45.
Davis, D.G., Perlman, M.E., and London, R.E.: 1994, *J. Magn. Reson.*, **B104**, 266–275.
Delaglio, F., Grzesiek, S., Vuister, G.W., Zhu, G., Pfeifer, J. and Bax, A.: 1995, *J. Biomol. NMR*, **6**, 277–293.
Deverell, C., Morgan, R.E. and Strange, J.H.: 1970, *Mol. Phys.*, **18**, 553–559.
Ferrage, F., Eykyn, T.R. and Bodenhausen, G.: 2000, *J. Chem. Phys.*, **113**, 1081–1087.
Ferrage, F., Eykyn, T.R. and Bodenhausen, G.: 2003, *ChemPhysChem.*, in press.
Frueh, D.: 2002, *Progr. NMR Spectrosc.*, **41**, 304–324.
Frueh, D., Tolman, J.R., Bodenhausen, G. and Zwahlen, C.: 2001, *J. Am. Chem. Soc.*, **123**, 4810–4816.
Grzesiek, S. and Bax, A.: 1992, *J. Magn. Reson.*, **99**, 201–207.
Helgstrand, M., Härd, T. and Allard, P.: 2000, *J. Biomol. NMR*, **18**, 49–63.
Ishima, R. and Torchia, D.A.: 1999, *J. Biomol. NMR*, **14**, 369–372.
Kay, L.E., Keifer, P. and Saarinen, T.: 1992, *J. Am. Chem. Soc.*, **114**, 10663–10665.
Kloiber, K. and Konrat, R.: 2000, *J. Biomol. NMR*, **18**, 33–42.
Kumar, A., Grace, R.C.R. and Madhu, P.K.: 2000, *Progr. NMR Spectrosc.*, **37**, 191–319.
Lienin, S.F., Bremi, T., Brutscher, B., Brüschweiler, R. and Ernst, R.R.: 1998, *J. Am. Chem. Soc.*, **120**, 9870–9879.
Lipari, G. and Szabo, A.: 1982, *J. Am. Chem. Soc.*, **104**, 4546–4559.
Logan, T.M., Olejniczak, E.T., Xu, R.X. and Fesik, S.W.: 1993, *J. Biomol. NMR*, **3**, 225.
Luz, Z. and Meiboom, S.: 1963, *J. Chem. Phys.*, **39**, 366–370.
Matlab: 1992, *Matlab Reference Guide*, Natick, MA.
Millet, O., Loria, J.P., Kroenke, C.D., Pons, M. and Palmer, A.G.: 2000, *J. Am. Chem. Soc.*, **122**, 2867–2877.
Mills, J.L. and Szyperski, T.: 2002, *J. Biomol. NMR*, **23**, 63–67.
Mulder, F.A.A., Skrynnikov, N.R., Hon, B., Dahlquist, F.W. and Kay, L.E.: 2001, *J. Am. Chem. Soc.*, **123**, 967–975.
Palmer, A.G., Cavanagh, J., Wright, P.E. and Rance, M.: 1991, *J. Magn. Reson.*, **93**, 151–170.
Pellecchia, M., Pang, Y.L.W., Kurochkin, A.V., Kumar, A. and Zuiderweg, E.R.P.: 1999, *J. Am. Chem. Soc.*, **121**, 9165–9170.
Pervushin, K.: 2001, *J. Biomol. NMR*, **20**, 275–285.
Sørensen, O.W., Rance, M. and Ernst, R.R.: 1984, *J. Magn. Reson.*, **56**, 527–534.
Vijay-Kumar, S., Bugg, C.E. and Cook, C.J.: 1987, *J. Mol. Biol.*, **194**, 531–544.
Vugmeyster, L., Perazzolo, C., Wist, J., Frueh, D. and Bodenhausen, G.: 2003, *J. Biomol. NMR*, in press.
Wennerström, H.: 1972, *Mol. Phys.*, **24**, 69–80.
Zidek, L., Stone, M.J. and Lato, S.M.: 1999, *Biochemistry*, **38**, 9850–9861.